ELSEVIER

Journal of Hydrology 255 (2002) 134–150

Journal of Hydrology

www.elsevier.com/locate/jhydrol

Overland flow to and through a segment of uniform resistance

Calvin W. Rose[a,*], William L. Hogarth[a], Hossein Ghadiri[a], Jean-Yves Parlange[b], A. Okom[a]

[a]*Faculty of Environmental Sciences, Griffith University, Nathan Campus, Nathan, Qld 4111, Australia*
[b]*Department of Agricultural and Biological Engineering, Cornell University, Ithaca, NY 14853, USA*

Received 4 January 2001; revised 20 August 2001; accepted 5 September 2001

Abstract

Recognising the utility of grass buffer strips in sediment retention, a fundamental hydraulic interpretation of flow through such strips is sought. In order to ensure reproducibility of results, a model porous resistive element consisting of beds of nails of various densities was used to simulate the hydraulic resistance offered by grass strips. In 14 experiments, the hydraulic consequences were measured for steady flow in a flume through nail beds of various densities at various flume slopes. A newly devised staining technique was used to measure the spatial variation in water depth to and through the resistive element. Provided nail density was not too low or slope too high, the maximum depth of water occurred as flow entered the nail bed. In such cases, momentum theory was able to provide a reasonably good prediction, both of the shape of the water profile within the nail bed, and of the slope and extent of the region of hydraulic adjustment formed upslope of the resistive element.

Keywords: Buffer strip; Filter strip; Momentum conservation; Overland flow; Hydrology

1. Introduction

The use of cross-slope vegetated strips as a soil conservation measure has attracted some scientific interest (Kemper et al., 1992). This interest has been accelerated by the need to reduce the amount of pollution in runoff to streams, leading to scientific study of the effectiveness of vegetated buffer strips in lessening the downstream impact of intensive land use (Landry and Thurow, 1997). Purpose-planted or reserved strips of pasture, referred to as grass buffer strips, is one method employed to reduce sediment or nutrient loading (Hairsine, 1996; Magette et al., 1989; Dabney et al., 1995; Munoz-Capena et al., 1999).

Experiments such as those described in the earlier references have demonstrated the effectiveness of even quite narrow continuous vegetated strips in leading to net deposition of sediment. It is recognised that the effectiveness of a flow-resistive element such as a strip of vegetation modifies the hydrology of overland flow, and that this modification has implications for transport and deposition of sediment and associated nutrients (Barfield et al., 1979; Flanagan et al., 1989; Dabney et al., 1995; Ghadiri et al., 2000, 2001). It is the hydraulic consequences for overland flow when it meets and flows through a resistive element which are examined in this study, which also follows Barfield et al. (1979) in using a resistive element consisting of rigid media in order to have reproducibility of results.

One common hydraulic consequence of flow meeting a buffer strip is the formation of a hydraulic jump and region of hydraulic adjustment upstream of the

* Corresponding author. Tel.: +61-7-3875-7397; fax: +61-7-3875-5282.
E-mail address: c.rose@mailbox.gu.edu.au (C.W. Rose).

0022-1694/02/$ - see front matter
PII: S0022-1694(01)00523-6

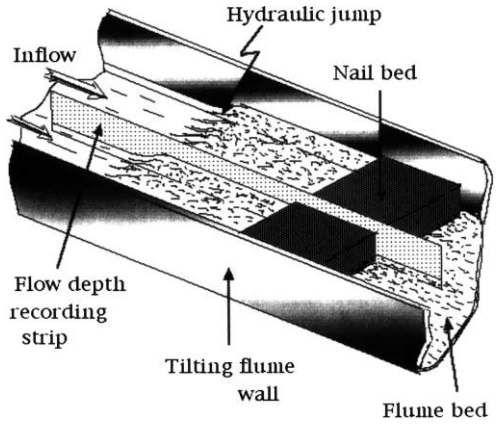

Fig. 1. The experimental arrangement for measuring depth of water flowing in a flume through a nail bed 0.2 m long in the direction of flow.

strip. There is a long history of investigation of hydraulic jumps in the hydraulic literature, where jumps have been induced to fulfil a variety of engineering objectives, such as the dissipation of flow energy (Chow, 1959). Engineering structures have been commonly designed to meet such objectives using momentum theory (Chow, 1959), and this type of theory will be employed in this paper.

Given the potential efficacy of a segment of flow-resistive medium in pollution reduction, it is most desirable to establish a sound basis for evaluating their likely effectiveness, and to aid their predictive design. This paper seeks to contribute to this objective by testing the ability of momentum theory to predict the hydraulic behaviour of flow through various resistive elements. This ability is tested by comparing prediction with a series of experiments with water flow over an impermeable surface placed at a variety of slopes, with flow passing through buffer strips of different but reproducible hydraulic resistance. The reproducible form of buffer strip adopted as suitable for the stated objectives is provided by dense arrays of regularly spaced steel nails. Such nail beds provide significant resistant to flow, as do strips of grass, and have the advantage over grass of yielding more reproducible results. Rigid nail beds suffer the disadvantage of not completely mimicking all the features of grass, such as its flexibility. However, it has been found that nail beds do provide a most useful and realistic simulation of the major hydraulic effects of grass strips (Ghadiri et al., 2000, 2001). Of course, there is no suggestion that nail beds are a practical replacement for vegetated buffer strips.

Since substantial sediment deposition is found to occur in the region of hydraulic adjustment formed by a buffer strip (e.g. Dabney et al., 1995; Ghadiri et al., 2000, 2001), the paper seeks in particular to be able to predict the extent of and flow velocity variation within this adjustment region.

2. Experimental methods

Experiments were carried out in a 1 m wide, 5.8 m long tiltable flume supplied with water of constant flow rate using a constant-head device. As described by Misra and Rose (1995), turbulence of water entering the tilting flume was greatly reduced by passage through a porous barrier of 1 cm diameter plastic tubes located at the flume inlet. The steady flux of water in these experiments was 2.27×10^{-3} m^3 m^{-1} s^{-1}. The flume was finished in marine ply, and flow resistive elements were fitted at a distance of 1.5 m from the flume exit. Buffer strip resistance to water flow down the flume was provided by a bed of uniformly spaced steel nails which filled the metre width of the flume and was of extent 0.2 m in the direction of flow (Fig. 1). Whilst nail diameter was constant at 3.76 mm, nail beds were constructed with three different regular nail spacings, giving nail densities (N) of 1600, 5150 and 10,200 nails m^{-2}, referred to hereafter as low density (LD), high density (HD), and very high density (VHD), respectively. Nails protruded 80 mm above the flume bed, well above the maximum water depth in any experiment (Fig. 1).

The steady depth of water in the impermeable flume increased following a hydraulic jump which signalled the commencement of a region of hydraulic flow adjustment that continued until flow entered the nail bed. The extent of the upstream influence of the nail bed on water level varied with the slope of the flume bed, and with nail density. Spatially continuous measurement of water depth over a length of 1 m was made using a flow depth recording strip located centrally within the flume bed and resting on it, the strip being parallel to the flow. This recording strip provided a measurement of water depth from 0.7 m upstream of the nail bed, within the nail bed, and

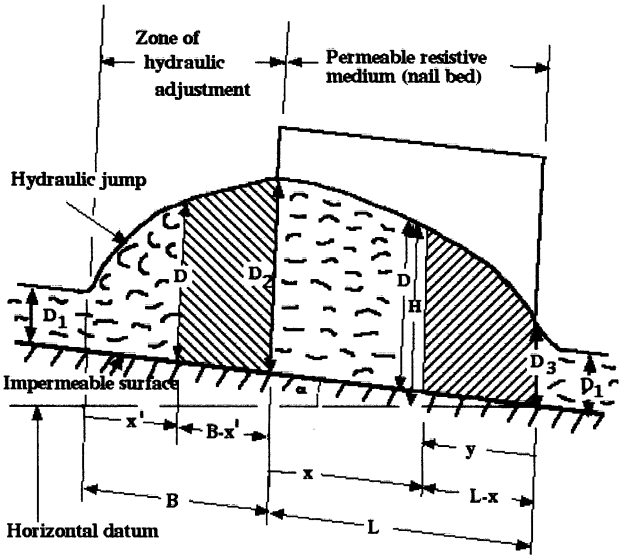

Fig. 2. Defining symbols used to describe steady flow over an impermeable surface to and through a segment of uniform resistive medium. See text for symbol definition.

0.1 m downstream of the bed (Fig. 1). The recording strip was cut from a 2 mm thick plastic sheet of Polyvinyl Chloride. The slightly expanded closed cell PVC had a silky semi-matt surface, and was manufactured by Forex (Product Code: Forex — E12.600). The leading edge of the strip was given a tapered or streamlined form to minimise flow disturbance. The strip was prepared for flow depth measurement by rubbing dry, finely ground potassium permanganate by hand into the strip surface using a cloth or paper applicator.

When a stable water-surface height has been achieved, the impregnated recording strip was placed vertically into the flow, being supported centrally in the nail bed (Fig. 1), so that it was normal to the flume bed on which it rested. Water dissolved the potassium permanganate in the measurement sheet so that, on it removal, an accurate permanent record of water level was recorded as a function of flow distance prior to, within, and following the nail bed. The apparent hairline accuracy of this record was compromised in part by recording the maximum height of minor surface waves. Close observation suggested that the effect of such waves were a more important source of error than the boundary layer bow waves produced by the streamlined leading edge of the 2 mm thick recording strip. No capillary rise effect due to surface tension was observable. Inaccuracy in water depth recording, partly due to surface waves, can be estimated from the variation in normal flow depth D_1 for the same slope where D_1 is defined in Fig. 2. Thus from Table 1, this error can be found to be approximately ± 0.1 cm, giving 20–10% accuracy in flow depth measurement of 1–2 cm, respectively. Once dried, this continuous record of water depth was photocopied and this record digitised using a specially developed in-house AUTOCAD program yielding a 1 m long record of water height at 2 mm intervals. Except for very low slope experiments, where the upslope hydraulic influence of the nail bed on water depth extended beyond the range of measurement, this measurement system yielded accurate spatially continuous data on water depth from where this depth was unaffected by the nail bed, through the region of hydraulic adjustment, the nail bed, and downslope of the nail bed, where after a short distance the water depth again became constant. On occasion plastic chips of a range of densities were introduced into the flow upstream of the hydraulic jump in order to visually investigate the nature of flow upstream and within the region of hydraulic adjustment.

3. Experimental results

In addition to measurement at equilibrium of flow

Table 1
Experimental data for the fourteen experiments together with derived quantities listed (S: fume slope; N: nail density; q: discharge rate per unit width; D_1: flow depth upstream of hydraulic jump; R_{e1}: Reynolds number: q/ν; F_{r1}: Froude number of upstream flow (Eq. (3)); D_2: water depth at entry to nail bed; D_3: water depth at exit from nail bed; D_{max}: maximum water depth (if $>D_2$); B: length of zone of hydraulic adjustment; e: distance between centres of adjacent nails; f: porosity (area of voids/frontal area) (Eq. (5)); R_d: nail matrix Reynolds number (Eqs. (6) and (7)); k: intrinsic permeability (Eq. (10))

Experiment	S (–)	N (nails m^{-2})	q (m^3 m^{-1} s^{-1})	D_1 (m)	R_{e1} (–)	F_{r1} (–)	D_2 (m)	D_3 (m)	D_{max} (if $>D_2$)	B (m)	e (m)	f (m^2 m^{-2})	R_d (–)	k (m^2)
Descriptor														
2HD[a]	0.01	5150	2.27×10^{-3}	7.18×10^{-3}	2.27×10^{3}	1.19	1.86×10^{-2}	1.26×10^{-2}		0.568	0.013935	0.7302	9.07×10^{2}	2.68×10^{-7}
2VHD	0.01	10,200	2.27×10^{-3}	NA	2.27×10^{3}	NA	2.42×10^{-2}	1.34×10^{-2}		NA	0.009901	0.6203		
2LD	0.0154	1600	2.27×10^{-3}	5.51×10^{-3}	2.27×10^{3}	1.77	1.41×10^{-2}	0.97×10^{-2}	1.51×10^{-2}	0.264	0.025	0.8496	1.02×10^{3}	4.05×10^{-7}
3HD[a]	0.0154	5150	2.27×10^{-3}	6.73×10^{-3}	2.27×10^{3}	1.31	1.85×10^{-2}	0.99×10^{-2}		0.36	0.013935	0.7302	9.28×10^{2}	2.49×10^{-7}
3VHD[a]	0.0154	10,200	2.27×10^{-3}	7.70×10^{-3}	2.27×10^{3}	1.07	2.33×10^{-2}	1.27×10^{-2}		0.636	0.0099901	0.6203	8.88×10^{2}	1.6×10^{-7}
3LD	0.034	1600	2.27×10^{-3}	5.37×10^{-3}	2.27×10^{3}	1.84	8.27×10^{-2}	1.11×10^{-2}	1.63×10^{-2}	0.035	0.025	0.8496	1.47×10^{2}	7×10^{-7}
4HD	0.034	5150	2.27×10^{-3}	5.60×10^{-3}	2.27×10^{3}	1.73	1.78×10^{-2}	1.24×10^{-2}	1.85×10^{-2}	0.072	0.013935	0.7302	9.99×10^{2}	2.08×10^{-7}
4VHD[a]	0.034	10,200	2.27×10^{-3}	5.10×10^{-3}	2.27×10^{3}	1.99	2.24×10^{-2}	1.29×10^{-2}		0.236	0.009901	0.6203	1.00×10^{3}	1.4×10^{-7}
4LD	0.052	1600	2.27×10^{-3}	6.20×10^{-3}	2.27×10^{3}	1.49	6.20×10^{-2}	1.25×10^{-2}	1.68×10^{-2}	0	0.025	0.8496	16.2×10^{3}	7.18×10^{-7}
5HD	0.052	5150	2.27×10^{-3}	5.20×10^{-3}	2.27×10^{3}	1.93	1.28×10^{-2}	1.30×10^{-2}	1.82×10^{-2}	0.022	0.013935	0.7302	1.30×10^{3}	2.86×10^{-7}
5VHD[a]	0.052	10,200	2.27×10^{-3}	4.60×10^{-3}	2.27×10^{3}	2.32	2.08×10^{-2}	1.21×10^{-2}		0.112	0.009901	0.6203	1.08×10^{3}	1.37×10^{-7}
6LD	0.0876	1600	2.27×10^{-3}	5.45×10^{-3}	2.27×10^{3}	1.80	5.40×10^{-2}	1.10×10^{-2}	1.23×10^{-2}	−0.01	0.025	0.8496	1.85×10^{3}	4.89×10^{-7}
6HD	0.0876	5150	2.27×10^{-3}	5.48×10^{-3}	2.27×10^{3}	1.79	6.20×10^{-3}	1.36×10^{-2}	2.12×10^{-2}	0.004	0.013935	0.7302	2.00×10^{3}	4.35×10^{-7}
6VHD	0.0876	10,200	2.27×10^{-3}	4.10×10^{-3}	2.27×10^{3}	2.76	1.14×10^{-2}	1.26×10^{-2}	2.96×10^{-2}	0.012	0.009901	0.6203	1.78×10^{3}	2.41×10^{-7}

[a] Indicates experiments used for theoretical analysis.

Fig. 3. Photograph looking vertically down on the hydraulic jump at the commencement of the region of hydraulic adjustment. The disturbed nature of flow is evident in at least the surface of the hydraulic jump. Flow is in the direction from uniform laminar flow to the disturbed flow.

depth as a function of distance, all experiments were photographed and observation made of the location of the transition from unimpeded flow down the flume to the hydraulic jump formed upstream of the nail bed.

Table 1 provides data for the range of experiments reported, with all symbols defined in Appendix A, and for convenience some are given in Table 1. The range of slopes (S), and nail densities (N) studied for the constant volumetric flow rate per unit width, or unit flow rate, q, of 2.27×10^{-3} m^2 s^{-1}, are also given in Table 1.

Fig. 2 illustrates the general features of some of the experiments. Both Figs. 2 and 3 indicate the presence of a hydraulic jump upslope of the nail bed. Since Chow (1959) has shown that the Froude number is the primary variable controlling the height and length of a classical hydraulic jump, Table 1 gives the Froude number of the upstream flow (F_{r1}). By definition,

$$F_{r1} = \frac{V_1}{(gD_1)^{1/2}} \tag{1}$$

where V_1 is the upstream flow velocity where flow depth is D_1, and g is the acceleration due to gravity.

Since the flume bed is impermeable, the discharge per unit width, q, is constant, and

$$q = DV \tag{2}$$

where D and V are general values of water depth and flow velocity.

From Eqs. (1) and (2), it follows that

$$F_{r1} = \frac{q}{D_1(gD_1)^{1/2}} \tag{3}$$

From Table 1, $F_{r1} > 1$ for all experiments, indicating supercritical flow upstream of the hydraulic jump.

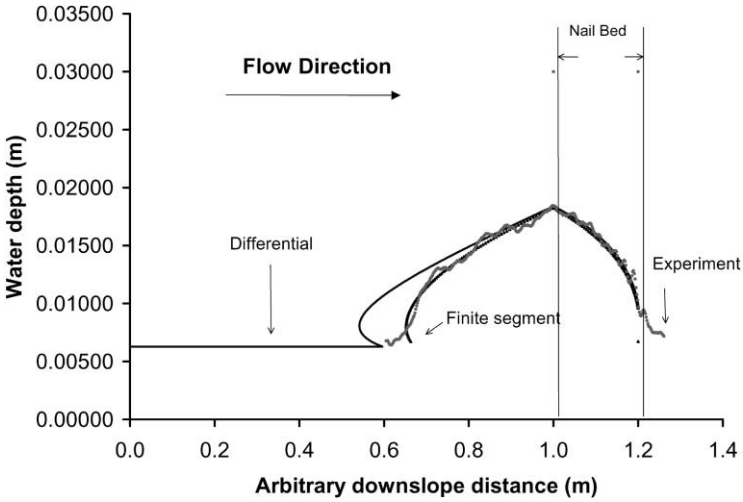

Fig. 4. Measurement results for steady water depth variation upstream and within a 0.2 m long high-density (3HD) nail bed with a bed slope of 1.54%. Measurement results are shown as a series of dots (●●●). Volumetric flow rate was 2.27×10^{-3} m^2 s^{-1} in all experiments. Profiles predicted with finite segment (▲▲▲) and differential theory (—) are also shown. The isolated point in line with the downstream end of the nail bed is the commencement point for the finite segment prediction of water depth. Flow direction is from left to right. Extent of nail bed is shown.

This flow characteristic would be due to the smoothness of the marine ply board surface of the flume. Replacing D_1 by D_2 in Eq. (3) shows that on entry into the nail bed, flow is subcritical, the distance B in Fig. 2 being a region of hydraulic adjustment. Comparison with the classic data on hydraulic jump characteristics given by Chow (1959) leads to the conclusion that the length B (Fig. 2) is usually greater than the length of the hydraulic jump, and that D_2 is greater than the expected alternate or sequent depth following the hydraulic jump. Thus it appears that there is a significant length of intermediate water surface between the end of the hydraulic jump and the beginning of the nail bed. The experimental data in Figs. 4, 6, 7(a) and (b) to be discussed in more detail later show that following the rapid depth increase characteristic of the hydraulic jump, the slope of this intermediate water surface is very approximately constant.

Since F_{r1} is mostly in the range 1.7–2.5 (Table 1), the hydraulic jump would be classed as 'weak' (Chow, 1959). On the nose of a weak hydraulic jump where depth is increasing downstream, Chow (1959) describes the water surface as bearing a series of small 'rollers'. When viewed from above, the photograph in Fig. 3 shows this feature as an intense cellular like flow structure which persists over the entire region of hydraulic adjustment formed by the presence of the nail bed.

The type of flow is also affected by its Reynolds number, R_e, and Table 1 gives upstream R_e as

$$R_{e1} = \frac{V_1 D_1}{\nu} = \frac{q}{\nu} \tag{4}$$

where ν is the kinematic viscosity of water. Table 1 shows R_{e1} to be about 2300, which places flow as being in the region where transition from a laminar to a turbulent nature can occur. Fig. 3 shows a very limited waviness of the flow surface upstream of the hydraulic jump. Upstream release of plastic chips of different densities indicate flow to be dominantly laminar in this region, but once the flow-transported chips reached the hydraulic jump their movements appeared chaotic and dispersive, bearing little relation to the general direction of flow. The smoothness of the marine ply board, which formed the surface of the flume, may have encouraged the laminar nature of flow prior to the hydraulic jump.

Summarising the data given in Table 1, Fig. 2 shows the depth of water at exit from the nail bed, D_3, to be a little greater than D_1. The decrease in water depth on exit from the nail bed back to the bed of the flume may indicate a hydraulic drop associated with a transition from subcritical flow in the nail bed to the supercritical flow on exit. (Since energy is dissipated in the hydraulic jump and drop sequence, the energy state immediately downslope of the nail element would not be as high as before the hydraulic jump, so the velocity would be slower, and water depth greater. Thus the return of water depth to D_1 would be gradual, as shown by measurement). Implications of the discrepancy between D_3 and D_1 will be considered in later sections of the paper.

Values of the length, B, of hydraulic transition given in Table 1 show that B varies with F_{ri} and slope, and this relationship will be studied further in Sections 4 and 5 of the paper.

Let d be the nail diameter, and e the nail spacing. Then the porosity of the nail bed, f, defined as the area of voids per unit frontal area, is given by

$$f = 1 - d/e \tag{5}$$

Table 1 shows that f increases from about 0.62 at VHD ($N = 10,200$ nails m^{-2}), to 0.85 at LD ($N = 1600$ nails m^{-2}).

The nature of interstitial flow through the bed of nails will be governed by the nail matrix (or cylinder) Reynold's number, R_d. This is defined as

$$R_d = \frac{q}{\nu}\left(\frac{d}{f D_m}\right) \tag{6}$$

where the mean depth during flow through the nail bed, D_m, is approximated (Fig. 2) by

$$D_m = (D_1 + D_2)/2 \tag{7}$$

Table 1 shows that in all experiments $R_d \gg 100$, indicating that flow through the interstices of the nail bed will be turbulent.

An important hydraulic characteristic of the nail bed is the intrinsic permeability of the nail matrix, k. The intrinsic permeability is related to the hydraulic conductivity, K, by

$$k = K\nu/g \tag{8}$$

Since the magnitude of R_d indicates turbulent flow through the nail bed it is strictly invalid to employ

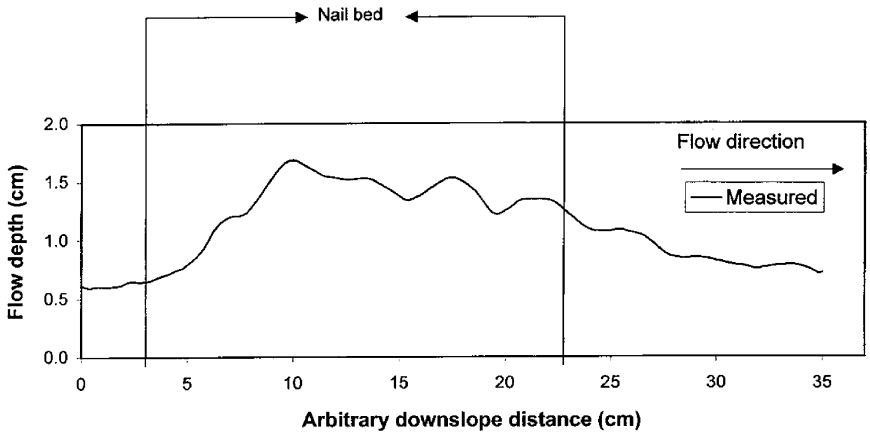

Fig. 5. Measurement results for steady water depth variation upstream and within a 0.2 m long low-density (4LD) nail bed with a slope of 5.2%.

Darcy's law in defining the hydraulic conductivity of the nail bed (Irmay, 1958). However, in order to obtain an order of magnitude estimate of k this objection will be ignored, and Darcy's law employed. For flow through the nail bed, the hydraulic conductivity is then defined using Darcy's equation as

$$q = \left(-K\frac{\mathrm{d}H}{\mathrm{d}x}\right)D \tag{9}$$

where H is the hydraulic head. From Fig. 2

$$H = D + (L + B - x)S$$

since x is taken positive downslope. Approximating $\mathrm{d}D/\mathrm{d}x$ by $(D_1 - D_2)/L$, and using an average value for D, it follows that the value of K can be approximated by

$$K = \frac{q}{\left(\frac{D_1 + D_2}{2}\right)\left(S - \frac{D_1 - D_2}{L}\right)} \tag{10}$$

With k calculated from Eqs. (8) and (10), Table 1 shows the order of magnitude of k is 10^{-7} m^2, a figure comparable with very coarse gravel (Freeze and Cherry, 1979). This also confirms that flow through the nail bed is likely to be turbulent, but Eqs. (9) and (10) will not be further used in the analysis.

Fig. 4 illustrates the type of results obtained for a slope (3.4%) and nail density (HD) intermediate within the density range covered (Table 1). In addition to the experimental data, two curves in Fig. 4 show predictions which will be discussed later. The experimental data in Fig. 4 clearly shows the effect of hydraulic adjustment upslope of the nail bed. The location where the increase in flow depth commenced was visually evident as well as being recorded by the dye trace record on the depth-measuring board. The extent of the hydraulic adjustment zone, denoted B in Fig. 2, depended on both slope and nail density. As the flume slope was increased over the range shown in Table 1, the extent of the adjustment zone decreased, and at the highest flume slope investigated (8.76%), except at VHD, no adjustment in flow depth occurred upslope of the nail bed, and the maximum water depth was well within the bed of nails.

The length of hydraulic adjustment, B, extended with increase in nail density from LD to VHD. At low nail density and slopes of 3.4% or greater, the maximum water depth took place, not at the upstream edge of the nail bed, where the maximum was D_2, but within the bed, as indicated by $D_{\max} > D_2$ in Table 1. This retreat of maximum flow depth into the nail bed was obvious at 5.2% slope or greater for HD, and at 8.76% for VHD.

The hydraulic adjustment length, B, was found to be approximately linearly related to the ratio N/S, with an $R^2 = 0.90$. The linear relationship was

$$B = 9.27 \times 10^{-7}(N/S) \tag{11}$$

Thus increasing nail density or decreasing slope both had the effect of increasing B.

Fig. 5 illustrates the retreat of the maximum water

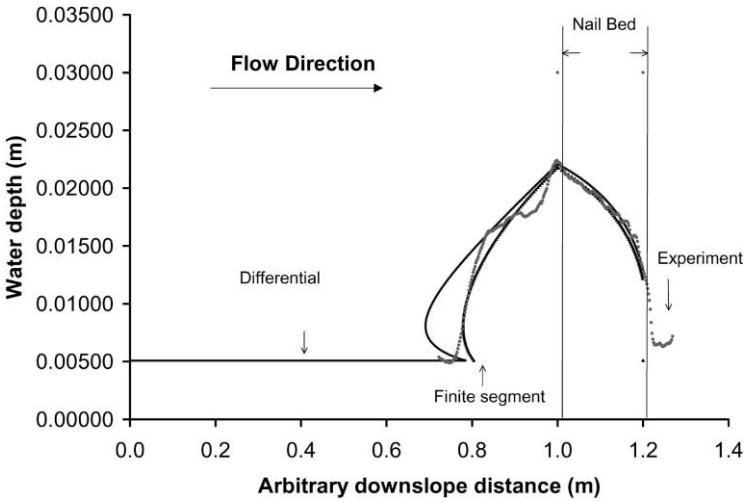

Fig. 6. Comparison (using symbols as in Fig. 4) of measured and predicted variation in water depth for flow through a 0.2 m long, high density (4VHD) nail bed at 3.4% bed slope.

height to within the nail bed, a feature associated with lower nail densities and higher slopes. This occurred in all but the five experiments given a symbol in the experiment descriptor column of Table 1. Detailed theoretical analysis is given later in this paper only for these five experiments in which the maximum water depth is D_2 located at the upstream nail face (Fig. 2).

The maximum water height penetrates the nail bed at higher slopes and lower nail densities presumably because under these conditions the full effect of the nail bed is not experienced by the flow until some flow penetration occurs. Theory for this type of experimental situation would be more complex than that given later in this paper.

Flow within the nail bed in Fig. 5 displays a pronounced waviness similar in nature to an undular jump sometimes associated with a hydraulic jump (Chow 1959). The less pronounced waviness shown in Fig. 4 has a wavelength approximately equal to nail spacing $e = 0.0139$ m (Table 1). Observation indicated that proximity of the recording board to a nail did result in a slight increase in recorded water height, providing a likely explanation of such waviness.

4. Theory for water flow to and through a resistive element

Theory is now developed designed to enable prediction of the results of water depth profiles measured in the zone of hydraulic adjustment and throughout the resistive element. There is particular interest in predicting the extent and depth or velocity profile in the zone of hydraulic adjustment because of its significance in the soil conservation context reviewed in Section 1. While Chow (1959) shows both Froude number and slope are involved in hydraulic jump behaviour, Eq. (11), which summarises the experimental results, indicates that in the context of these experiments the character of the flow-resistive element also plays a significant role in the behaviour of the hydraulic adjustment effect generated by its presence. Flow, both in the zone of hydraulic adjustment and through the nail bed, is indicated as turbulent (see Fig. 3 and comment on R_d and k in Table 1). Despite possible limitations, momentum conservation will be used in developing the theory.

In applying momentum conservation, a significant force term is the component of the weight of water acting down the flume. This force component clearly requires information on the water surface profile, which in a predictive context is unknown. To overcome this problem it is commonly assumed that recourse must be made either to experiment or to assumptions in order to apply momentum conservation (Chow, 1959; Henderson, 1966; French, 1985). This paper will show how this problem can be overcome, at least approximately.

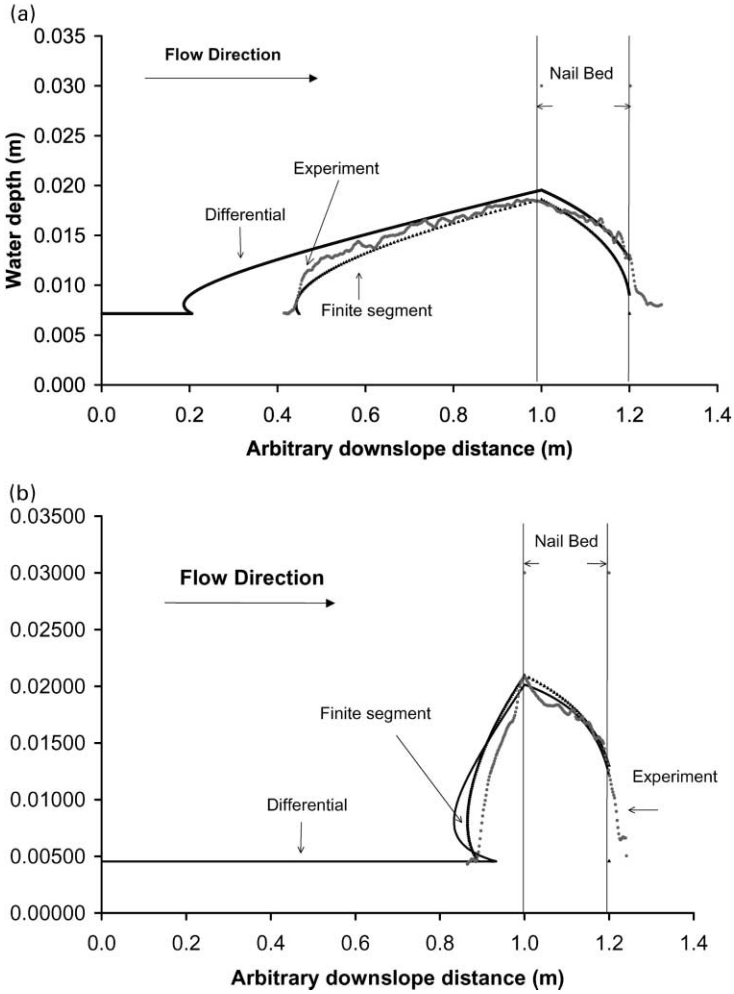

Fig. 7. Comparison (using symbols as in Fig. 4) of measured and predicted variation in water depth for flow through a 0.2 m long resistive element for (a) a high density (2HD) nail bed at a low slope of 1%, and (b) a very high density (5VHD) nail bed at a higher slope of 5.2%.

Theory will be developed commencing with flow at exit from the nail bed resistive element, and working upstream through this element to predict depth D_2 (Fig. 2). This predicted value of D_2 will then be used to predict the profile shape of the zone of hydraulic adjustment, and its extent, B (Fig. 2).

As indicated in Table 1, and in Figs. 6 and 7, the water depth at exit from the nail bed, D_3, is a little greater than the normal depth D_1, and likely reasons for this were given in Section 3. Analysis is commenced at the downslope end of the nail bed by taking D equal to its measured value D_3, or alternatively by assuming $D = D_1$. Whilst prediction of the water depth profile in the nail bed would be expected to be more accurate taking $D = D_3$, the advantage of assuming $D = D_1$ is that D_1 is known, being the normal depth (Fig. 2).

A parameter in the theory is the drag coefficient, C_d, of an individual nail. The appropriate value of C_d was obtained using momentum conservation considerations now developed.

4.1. Theory for the prediction of water depth within the nail bed using finite segments

Denote the volumetric water content within the nail

bed by θ, where $\theta < 1$. Then unit flow rate q is given by

$$q = \theta VD \tag{12}$$

Consider the finite segment of flow within the nail bed between x and $x = L$, of length $(L - x)$ and shown shaded on the right hand side of Fig. 2. Prediction will commence at the end of the nail bed and work upslope, and the upslope direction with origin at $x = L$ will be denoted by y (Fig. 2).

The momentum change for flow across the segment from $y = 0$ to y will depend on three different types of forces. Firstly there is the component of the weight of water, W, in the segment, which acts down the plane. This component is $W \sin \alpha$ or WS, where, using the average water depth $D_a = (D_3 + D)/2$ for the segment, W is given by

$$W = \theta \rho g D_a y \tag{13}$$

The second force arises from the net static pressure acting down the plane, and is given by $(\rho g \cos \alpha/2)(D^2 - D_3^2)$, a positive quantity since $D > D_3$ (Fig. 2). Finally the nail bed offers a resistance acting in the upslope direction to oppose the flow. The drag force, F, due to flow round an object presenting a cross-sectional over A to the flow, and with drag coefficient C_d, is given by

$$F = (1/2)\rho V^2 A C_d \tag{14}$$

where for a single cylindrical nail of diameter d, in flow depth D

$$A = dD \tag{15}$$

For a nail bed of width 1 m and length y, the drag force with nail density N (m^{-2}) will be

$$F = (1/2)\rho V_a^2 d D_a C_d N y \tag{16}$$

where D_a and V_a are the average water depth and velocity in the segment.

The resistance to flow offered by the flow bed will be neglected, being small compared to that offered by the bed of nails.

Momentum conservation for the segment of length y shown shaded within the nail bed on the right of Fig. 2 then requires that

$$\rho q(V_3 - V) = \theta \rho g D_a S y + \frac{\rho g \cos \alpha}{2}(D^2 - D_3^2) - (1/2)\rho V_a^2 d D_a C_d N y \tag{17}$$

with flow velocity and depth related as in Eq. (12). For all experiments the value of 1.7 for C_d in Eq. (17) gave good prediction of both D_2 and the water depth profile within the nail bed. This value of 1.7 for C_d is significantly higher than the drag coefficient for an isolated smooth cylinder, which is close to 1.0 within the relevant Reynold's number range of 900–2000 (Table 1) (Marks, 1951). The higher value of C_d used to match the experimental data may due to theoretical limitations and to the possibility that the complex turbulent flow through the nail bed may yield higher values of C_d than for an isolated cylinder.

The theory in Eq. (17) uses V_3 and D_3, the measured values at exit from the nail bed. From a predictive standpoint it would be preferable for V_3 and D_3 to be replaced by V_1 and D_1 which are known, being the normal flow values. Interestingly, it was found that the predictions of water profile depth using Eq. (17) were altered very little by this replacement. Hence, all the results presented for the finite segment form of theory in Figs. 4, 6 and 7 commence assuming $D = D_1$ at exit from the nail bed, and that C_d is constant at 1.7. As can be seen in these figures there is good agreement between measurement and momentum conservation predictions based on the finite segment form of expression. Thus, prediction with this form of theory is quite good even without knowledge of D_3.

Eq. (17) was solved for the value of y when D was increased incrementally from D_1, allowing D to be plotted as a function of y to give the calculated water surface profile within the nail bed.

4.2. Differential theory for the prediction of water depth within the nail bed

In Eqs. (13) and (16), average values, D_a and V_a, of depth velocity had to be used because the shape of the water profile is not known prior to the solution of Eq. (17) for D. Good agreement between measured and predicted profiles indicates that the approximation involved in the use of average values is quite acceptable. Evidently, the error introduced by use of

average values is small because the departure of the profile from linearity is modest. However, even this modest error can be eliminated by expressing momentum conservation in differential form and solving the resulting differential equation numerically.

The differential form of Eq. (17) is

$$-\rho q \, \mathrm{d}V = \theta \rho g D S \, \mathrm{d}y + \rho g \cos \alpha D \, \mathrm{d}D - \rho \frac{V^2}{2} dD C_\mathrm{d} N \, \mathrm{d}y \quad (18)$$

if $y \, \mathrm{d}D$ is neglected compared to $D \, \mathrm{d}y$.

Now from Fig. 2,

$$y = L - x,$$

and so

$$\frac{\mathrm{d}y}{\mathrm{d}x} = -1 \quad (19)$$

From Eqs. (18) and (19),

$$-q \frac{\mathrm{d}V}{\mathrm{d}x} = -\theta g D S + g \cos \alpha D \frac{\mathrm{d}D}{\mathrm{d}x} + \frac{V^2}{2} dD C_\mathrm{d} N \quad (20)$$

From Eq. (12),

$$q \frac{\mathrm{d}V}{\mathrm{d}x} = -\frac{q^2}{\theta D^2} \frac{\mathrm{d}D}{\mathrm{d}x} \quad (21)$$

Substituting from Eq. (21) in Eq. (20) and re-arranging leads to the following differential equation for D:

$$\frac{2}{D} \frac{\mathrm{d}D}{\mathrm{d}x} = \frac{2gSD^2\theta^2 - q^2 dC_\mathrm{d} N/\theta}{g\theta D^3 \cos \alpha - q^2} \quad (22)$$

The result of numerical solution of this equation for D as a function of x, commencing with $D = D_3$ at exit from the nail bed, is shown in Figs. 4, 6, 7(a) and (b), where good agreement with measurement within the nail bed is indicated. The single value of 1.85 used for C_d in Eq. (22) was found to give the quite good agreement between measured profiles of water depth and those predicted using differential theory. This value of C_d, (1.85), is higher than the value of 1.7 chosen for the finite element theory.

For both the finite segment (Eq. (17)), and differential forms (Eqs. (18) and (22)) of expressing momentum conservation, the predicted values of D_2 were then used as input to momentum conservation analysis of the region of hydraulic adjustment upslope of the nail bed, of extent B (Fig. 2). This analysis is given in the following sections.

4.3. Finite segent theory for predicting the extent and depth profile of the zone of hydraulic adjustment

Texts such as Chow (1959), Henderson (1966) and French (1985) consider hydraulic jumps in an engineering context where the cause of the jump is different from the presence of a resistive element, and where interest lies in issues such as energy dissipation and prediction of the depth ratio corresponding approximately to D_2/D_1 in Fig. 2. This literature emphasises the importance of Froude number and slope to broad aspects of jump geometry, but appears less interested in the velocity profile of the jump, which is an issue of significance in soil conservation contexts, as noted in the Introduction.

French (1985) advises that one of the primary difficulties in quantitatively applying momentum conservation is in defining the weight of water component, a problem dealt with qualitatively by Chow (1959) through the introduction of a 'shape factor'. Henderson (1966) states that "in the end result recourse must be had to experiment, which alone can determine the profile of the jump and hence the weight of water…"

Measured profiles of water depth in the zone of hydraulic transition, (such as in Fig. 4), are encompassed within the two assumptions of, firstly, a linear profile from D_2 to D_1 at the hydraulic jump commencement, and secondly, the alternative assumption that depth is constant at D_2 within the transition zone, falling abruptly to D_1 at the hydraulic jump. Data from this paper, and general experience (Chow, 1959), suggests that the second assumption of a constant D_2 is closer to reality and gives better prediction. Finite segment theory is developed making this simplification in the weight component term, but not in other terms. Theory was also developed for the alternative assumption of a linear water surface profile in expressing the downslope weight of water force component, and the consequences of this will be discussed later.

Despite the substantial energy loss associated with the recirculating roller structure in the hydraulic jump (Fig. 3), the paper examines the consequences of prediction based solely on the principles of continuity and momentum conservation. Consider application of

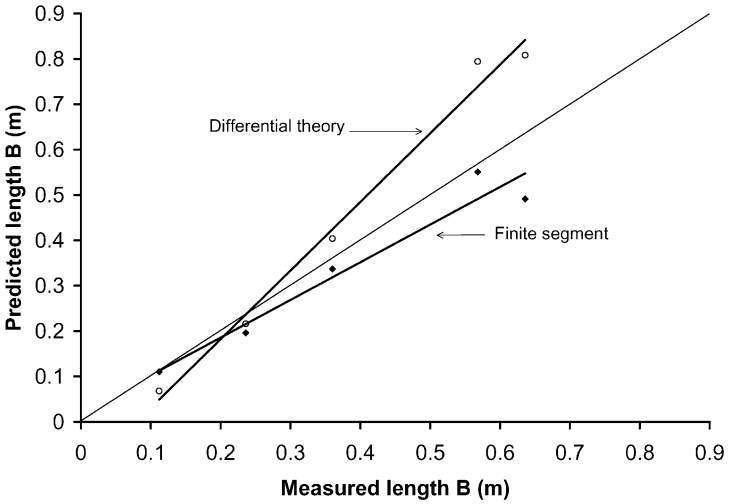

Fig. 8. Comparison of the measured length of the hydraulic adjustment zone, B (Fig. 2), with B predicted from momentum theory using either (i) a finite segment form (Eq. (25)) with D_2 predicted using (Eq. (17)), or (ii) using a differential theory form (Eq. (30)) with D_2 predicted using (Eq. (22)). Predicted values are shown fitted with linear relationships and compared to a 1:1 line.

momentum conservation to the cross-hatched volume of length $(B - x')$ in Fig. 2, where this volume extends upslope from the commencement of the nail bed, and where $x' = 0$ denotes commencement of the hydraulic jump. Since the flume surface was smooth, the resistance offered to flow over that surface is neglected compared to the net force due to static pressure differences at either end of the volume, and the downslope component of the weight of water in the volume. With the stated assumptions, momentum conservation for the segment requires that

$$\rho q(V_2 - V) = \frac{\rho g}{2}(D^2 - D_2^2)\cos\alpha + D_2\rho g S(B - x') \tag{23}$$

Noting that $q = D_2V_2 = DV$, it follows from Eq. (23) that

$$(B - x') = \frac{q^2}{gD_2S}\left(\frac{D - D_2}{D_2D}\right) - \frac{1}{2D_2S}(D^2 - D_2^2)\cos\alpha \tag{24}$$

Commencing with $D = D_2$ (for which $(B - x') = 0$), progressively smaller values of D than D_2 were inserted into the right-hand side of Eq. (24) to yield the corresponding value of $(B - x')$. This was continued until D was equal to D_1, thus defining the length, B, of the zone of hydraulic adjustment (Fig. 2). In this way, prediction of the profile of water depth (and so velocity) in the adjustment zone was achieved.

When $x' = 0$, $D = D_1$ by definition, and the predicted length B is then available from Eq. (24) as

$$B = \frac{(D_2 - D_1)}{D_2S}\left[\frac{(D_1 + D_2)}{2}\cos\alpha - \frac{q^2}{gD_1D_2}\right] \tag{25}$$

A comparison of predicted and measured lengths of hydraulic adjustment zones is given in Fig. 8, indicating reasonable agreement.

As is illustrated in Fig. 4, calculation of D using Eq. (24) typically overshoots the length B as calculated using Eq. (25), with calculated water depth reduced to D_1 in an inverted and unrealistic manner. This may be interpreted as indicating a hydraulic shock commencing at $x' = 0$, but the unrealistic predicted overhanging 'nose' of water is evidently due to inadequate assumptions or deficiency in the theory.

The assumption, made for the sole purpose of estimating the downslope weight of water component, that the depth of water in the zone of hydraulic adjustment was constant at D_2, is clearly not accurate. However making an alternative assumption of a linear shape from D_2 to D_1 in calculating the weight component term leads to a predicted surface profile shape which is also almost linear, and yields predicted values of B some two to three times measured values.

4.4. Differential theory for predicting the extent and depth profile of the zone of hydraulic adjustment region

The differential form of the segment momentum conservation Eq. (23) is

$$q\frac{\mathrm{d}V}{\mathrm{d}x'} = gDS - g\cos\alpha D\frac{\mathrm{d}D}{\mathrm{d}x'} \tag{26}$$

with

$$q = VD \tag{27}$$

Dividing Eq. (26) by D, using Eq. (27), and noting that

$$\frac{\mathrm{d}}{\mathrm{d}x'}(V^2) = 2V\frac{\mathrm{d}V}{\mathrm{d}x'}$$

then Eq. (26) becomes

$$\frac{1}{2}\frac{\mathrm{d}}{\mathrm{d}x'}(V^2) = gS - g\cos\alpha\frac{\mathrm{d}D}{\mathrm{d}x'} \tag{28}$$

Integration of Eq. (28) from x' to $x' = B$ (Fig. 2), and using Eq. (27) leads to

$$S(B - x') = \left(\cos\alpha D_2 + \frac{q^2}{2gD_2^2}\right) - \left(\cos\alpha D + \frac{q^2}{2gD^2}\right) \tag{29}$$

allowing x' to be solved if D is decreased incrementally from D_2.

By definition, when $x' = 0$, $D = D_1$, yielding the length, B, from

$$SB = \left(\cos\alpha D_2 + \frac{q^2}{2gD_2^2}\right) - \left(\cos\alpha D_1 + \frac{q^2}{2gD_1^2}\right) \tag{30}$$

Fig. 8 compares the differential form predictions of B using Eq. (30) with both the measured value of B (given by the 1:1 line), and B predicted using the finite segment form of expression (Eq. (25)). Differences in prediction result from differences between Eqs. (24) and (29) and consequent differences between Eqs. (25) and (30) for B. The differential form of momentum conservation expression has the following two theoretical advantages over the finite segment theory of Section 4.3

(i) No á priori approximation is required concerning the profile shape of the zone of hydraulic adjustment in order to describe the component of the weight of the water acting down the plane. In this sense, the differential theory is more fundamental than the finite element form.
(ii) An analytical solution of the differential Eq. (26) is possible (Eq. (29)).

Despite these two advantages, whether or not the differential theory leads to better prediction of the profile shape and length of the zone of hydraulic adjustment will be considered in Section 5.

5. Model testing and discussion

Fig. 4 gives results for experiment 3HD of both water profile measurement and prediction using the two forms of momentum theory and their attendant assumptions given in Section 4. Figs. 6 and 7 provide a similar comparison of measurement and prediction for three other experiments for which the maximum measured water height was at the commencement of the resistive element, as was the case for those experiments listed with a symbol in Table 1.

In a fully predictive context the height of the water at exit from the nail bed, D_3, would not be known. The finite segment theory generally coped well simply assuming that the exit water depth is given by the (known) normal depth D_1. As shown in Figs. 4, 6, and 7(b), a rather sudden upstream increase in predicted water depth resulted with this assumption. Agreement in trend, and reasonable agreement in magnitude between measured and water depths predicted using finite element theory within the nail bed is shown in all Figs. 4, 6 and 7.

The predicted values of D_2 and B increased somewhat as the value assumed for the drag coefficient C_d increases. For finite segment theory this sensitivity of D_2 and B to the value adopted for C_d was investigated by repeating the calculations with C_d increased from 1.7, (the value used in the results presented), to 2.2, an increase of 0.5. Sensitivity is expressed by the change in D_2 or B per unit increase in C_d. The increase in D_2 per unit increase in C_d fell slightly from 4×10^{-3} m for 5HD to 3×10^{-3} m for 2HD. The corresponding increase in B ranged from 0.048 m for 5VHD to 0.18 m for 2HD, the sensitivity increasing with decrease in slope.

If prediction using the differential form of momentum conservation expression was commenced assuming $D_3 = D_1$ at exit from the nail bed, a substantially higher value of C_d had to be employed in order to obtain agreement with the measured value of D_2 (Fig. 2). Also the predicted water profile shape was then substantially below that of the measured profile, and different to the predicted profiles shown in Figs. 4, 6, and 7 where differential theory calculations always commenced with depth at exit from the nail bed $= D_3$, the measured value.

Thus the differential form of momentum conservation expression, for reasons that need more investigation, differ in behaviour from the finite segment form of expression, which is rather indifferent to the exit value of D used to commence the calculations.

The formation of a shock or hydraulic jump at the commencement of the zone of hydraulic adjustment is the result of a transition from supercritical to subcritical flow. Fig. 3 illustrates the intense cellular or eddy flow structures within the zone of hydraulic adjustment. Such structures may lead to dissipation of momentum, so that momentum conservation may be expected to describe only the general features of depth profiles in the zone of hydraulic adjustment. The observed nature of the hydraulic jump was generally consistent with the description of a weak hydraulic jump by Chow (1959).

Figs. 4, 6 and 7 show that agreement between predicted and measured profiles of water depth in the zone of hydraulic adjustment was reasonable, but not as good as within the nail bed. As shown in Figs. 4 and 7(a), discrepancies are significant for the differential form of theory given in Section 4.4. The assumption concerning a constant water surface profile made in order to express the downslope weight of water component in the finite segment form of momentum conservation mostly yielded better agreement with measurement than the differential form. This constant depth assumption has more effect on predictions in the zone of hydraulic adjustment than did the use of average depth values within the nail bed, for the following two reasons. Firstly the implied linear depth approximation is more realistic within the nail bed, and secondly the large resistance offered by the nail bed reduces the significance of any assumption made in describing the downslope weight component term.

A consistent peculiar feature in the predicted water profile shape in the hydraulic adjustment zone using either momentum conservation theory is the re-entrant form at the nose or commencement of the hydraulic jump illustrated in Figs. 4, 6 and 7. Presumably this feature is one outcome of limitations in the momentum conservation expressions used.

Figs. 4, 6–8 show that Eq. (25) of the finite segment theory gives reasonably good prediction of B, with D_2 predicted using Eq. (17) with $y = L$ and assuming $D_3 = D_1$. As would be expected, prediction of B is more accurate if the measured value of D_2 is used rather than the predicted value (results not shown). Fig. 8 shows that Eq. (30), based on the differential form of momentum conservation expression, may not give quite as accurate a prediction of larger values of length B as does the finite segment form of expression. This is despite the fact that for the first time Eq. (30) provides an analytical solution of the extent and profile shape of the zone of hydraulic adjustment, without requiring either use of a shape factor (Chow, 1959), or involving a simplification, as is necessary in the finite segment form of momentum conservation described in this paper.

Samuels (1989) developed a simple approximate perturbation solution to the St Venant equation, designed to allow estimation of backwater lengths in rivers. However, the equation of Samuels (1989) was found to overestimate substantially the value of B in the reported experiments. It follows that gradually varied steady flow theory is unable to adequately explain the measurements in these experiment involving a hydraulic jump and flow adjustment.

An empirical relationship for the experiments reported (with $R^2 = 0.90$) was given previously in Eq. (11):

$$B = 9.27 \times 10^{-7}(N/S)$$

Eq. (11) has general theoretical support from Eq. (25), which indicates an inverse dependence on S; also the difference in water height, $(D_2 - D_1)$ in Eq. (25), will increase with N.

A corresponding empirical relation for the values of D_2 reported in Table 1 is given (with $R^2 = 0.62$) by

$$D_2 = 0.0159 + 1.92 \times 10^{-5}(D_1 + SL)N \text{ (m)} \qquad (31)$$

The presence of N in Eq. (31) indicates an effect

associated with the hydraulic conductivity of the resistive medium.

We also seek a description of the velocity profile in the zone of hydraulic adjustment shown by Dabney et al. (1995), Ghadiri et al. (2000, 2001) to be important in the deposition of sediment in front of grass hedges. This shape can be well predicted using Eq. (24). However in order to avoid the numerical solution involved, the following empirical equation for velocity V as a function of x fits the data quite well, with D_2 given by Eq. (31) and B by Eq. (11)

$$V = V_1(D_1/D_2)^{(x/B)^{0.5}} \tag{32}$$

The sudden rise in water depth associated with the hydraulic jump was quite visible in itself, and the photographic record confirmed visual evidence that following the shock or hydraulic jump, turbulence commenced and continued through the entire hydraulic adjustment zone (Fig. 3). A stream of near-buoyant plastic chips submitted to the laminar stream upslope of the jump underwent chaotic and apparently rotational motions on reaching the hydraulic jump. Also, an added dye trace, which continued with uniform width in the laminar flow supercritical region upslope of the jump, suddenly commenced a continuous expansion in width on reaching the hydraulic jump, adding further evidence supporting the turbulent nature of flow in the zone of hydraulic adjustment. Fig. 3 appears to indicate more developed rollers or cellular turbulence than would be expected at these low Froude numbers from sketches given in Fig. 15-2 of Chow (1959). Turbulence was also in evidence downstream of the nail bed.

Fig. 5 illustrates a feature which was common to varying degrees in all those experiments listed without a star in Table 1. This common feature was that the maximum water depth occurred some distance into the nail bed, and not at its leading edge. This feature was characterised in Table 1 by $D_{max} > D_2$. Nails were placed in a square pattern in all experiments, so that at the lowest nail density (LD), the distance between adjacent nail centres was $(1/\sqrt{1600})m = 2.5$ cm. Flow between adjacent pairs of nails therefore may need to penetrate some distance into the nail bed before experiencing the full effect of flow resistance characteristic of the particular nail density.

6. Conclusion

Fourteen experiments with constant water flow rate to and through a constructed resistance element consisting of a nail bed were used to simulate flow through a vegetated buffer strip. The hydraulic adjustment zone formed upslope of the resistive element with supercritical inflow had characteristics which depended on the slope of the flow (S), and on the hydraulic resistance of the element as indicated by variation in nail density (N). Over the experimental range investigated, the extent of the zone of hydraulic adjustment was approximately proportional to the ratio N/S, and was reasonably well predicted by momentum theory (Fig. 8). Experiment and photography showed the zone of hydraulic adjustment was initiated by a hydraulic jump exhibiting a highly disturbed and possibly cellular or recirculating structure, sometimes referred to as rollers. Flow through the nail bed was also indicated as turbulent.

Using a newly devised staining technique, the equilibrium depth of water for each experiment was recorded from prior to the hydraulic jump, through the hydraulic adjustment zone and nail bed and beyond, to an accuracy of approximately ± 1 mm. At higher slopes and lower nail densities the maximum height of flow occurred some distance into the nail bed. In other circumstances the maximum height was recorded as flow entered the nail bed, and in these cases detailed analysis of the profiles of water was carried out.

This analysis was carried out using momentum theory for free surface flows, first applied to flow through the nail bed in order to experimentally confirm a value for the drag coefficient of an individual nail, which was approximately constant despite variation in nail density. Application of momentum theory in finite segment form was commenced with flow at exit from the nail bed, where for simplicity the normal depth of flow on the flume was assumed in prediction. This theory was found to provide a good prediction of water depth throughout the resistive element. The predicted water depth at entry to the resistive element was then used to predict the profile shape and extent of the zone of hydraulic adjustment, using different momentum theory appropriate to that region.

In addition to this finite segment form of expression

of momentum conservation, a differential form was also employed, both within the nail bed, and in the flow adjustment zone upslope of the nail bed. Both forms of momentum theory expression led to virtually identical results within the nail bed. In the zone of hydraulic adjustment, however, the more approximate finite segment expression form of momentum conservation generally yielded more accurate predictions than did the more fundamental differential expression of momentum conservation. However, the more fundamental differential form allowed analytical expression of hydraulic behaviour, and removed the need for simplification required in the finite element form.

Despite conceptual reservations concerning the predictive adequacy of continuity and momentum conservation principles alone, especially in the zone of hydraulic adjustment following the hydraulic jump, useful agreement with measured flow depth profiles was obtained in the five experiments susceptible to such analysis.

This paper contributes to the ability to predict the likely hydrologic performance of designed buffer strips with supercritical inflow, at least over a range of slopes up to about 9%, and assuming the buffer strip is not completely submerged by the flow.

Acknowledgements

The assistance of Mr Aubrey Chandica with the AutoCAD operation and a Griffith University research grant for funding to undertake this research is gratefully acknowledged. The authors also wish to thank referees for very useful and helpful comments.

Appendix A

Table A1.

Table A1
List of symbols

Symbol	Description	Defining equations/figures
Roman		
A	Immersed cross-sectional area of a single nail	Eq. (15)
B	Length of zone of hydraulic adjustment	Eqs. (11), (25) and (30), Fig. 2
C_d	Drag coefficient of a single nail	
d	Nail diameter	
D	Depth of water flow	
D_1	Depth of normal flow	Fig. 2
D_2	Depth of water at entry to the nail bed	Fig. 2
D_3	Depth of water of exit from the nail bed	Fig. 2
D_a	Average water depth over distance $(L-x)$ or y	Fig. 2
D_m	Approximate mean water depth for flow through the nail bed	Eq. (7)
e	Nail spacing	
f	Porosity of the nail bed	Eq. (5)
F	Drag force on flow exerted by a segment of the nail bed	Eq. (16)
F_{r1}	Froude number of upstream normal flow	Eqs. (1), (3)
g	Acceleration due to gravity	
H	Hydraulic head	Fig. 2
k	Intrinsic permeability of the nail bed	Eq. (8)
K	Hydraulic conductivity of the nail bed	Eq. (10)
L	Length of nail bed	Fig. 2
N	Nail density (no. nails m^{-2})	
q	Unit discharge	Eq. (2) (outside nail bed) Eq. (12) (for nail bed)
R_d	Nail matrix Reynold's number	Eq. (6)
R_{el}	Reynold's number for flow	Eq. (4)
S	Bed slope $= \sin\alpha$	
V	Velocity of flow	
V_1	Flow velocity with flow depth D_1	

Table A1 (*continued*)

Symbol	Description	Defining equations/figures
V_2	Flow velocity with flow depth D_2	
V_a	Average flow velocity over distance $(L - x)$ or y	Fig. 2
W	Weight of water in defined segment	Eq. (13)
x	Downslope distance measured from upstream face of the nail bed	Fig. 2
x'	Downslope distance measured from the commencement of the hydraulic jump	Fig. 2
y	Distance measured upslope from the downslope of the nail bed	Fig. 2
Greek		
α	Slope angle of the flow bed	Fig. 2
θ	Volumetric water content of flow within the nail bed	
ν	Kinematic viscosity of water	
ρ	Water density	

References

Barfield, B.J., Tollner, E.W., Hayes, J.C., 1979. Filtration of sediment by simulated vegetation. I. Steady-stage flow with homogenous sediment. Transactions of ASAE 22 (5), 540–545 also see p. 548.

Chow, V.T., 1959. Open Channel Hydraulics. McGraw Hill, New York.

Dabney, S.M., Meyer, L.D., Harmon, W.C., Alonso, C.V., Foster, G.R., 1995. Depositional patterns of sediment trapped by grass hedges. Transactions of ASAE 38 (6), 1719–1729.

Flanagan, D.C., Foster, G.R., Neibling, W.H., Burt, J.P., 1989. Simplified equations for filter strip design. Transactions of ASAE 32 (6), 2001–2007.

Freeze, R.A., Cherry, J.A., 1979. Groundwater. Prentice Hall, Englewood Cliffs, NJ.

French, R.H., 1985. Open-Channel Hydraulics. McGraw Hill, New York.

Ghadiri, H., Hogarth, W.L., Rose, C.W., 2000. The effectiveness of grass strips for the control of sediment and associated pollutant transport in runoff. In: Stone, M. (Ed.). Role of Erosion and Sediment Transport in Nutrient and Contaminant Transfer. IAHS Publication No. 263, Oxfordshire, UK, pp. 83–91.

Ghadiri, H., Rose, C.W., Hogarth, W.L., 2001. The influence of grass and porous barrier strips on runoff hydrology and sediment transport. Transactions of ASAE. 44 (2).

Hairsine, P.B., 1996. Comparing grass filter strips and near-natural riparian forests for buffering intense hillslope sediment sources. Proceedings of the First National Conference on Stream Management in Australia, 19–23 February 1996, Merrijig, Australia. Cooperative Research Centre for Catchment Hydrology, Monash University, Victoria, Australia pp. 203–206.

Henderson, F.M., 1966. Open Channel Flow. Macmillan, New York.

Irmay, S., 1958. On the theoretical derivation of Darcy and Forchheimer formulas. Transactions, American Geophysical Union 39, 702–707.

Kemper, D., Dabney, S., Kramer, L., Dominick, D., Keep, T., 1992. Hedging against erosion. Journal of Soil and Water Conservation 47, 284–288.

Landry, M.S., Thurow, L.L., 1997. Function and design of vegetation filter strips: An annotated bibliography. Texas State Soil and Water Conservation Board Bulletin No. 97-1. P.O. Box 658, Temple, USA, p. 67.

Magette, W.L., Brinsfield, R.B., Palmer, R.E., Wood, J.D., 1989. Nutrient and sediment removal by vegetated filter strips. Transactions of ASAE 32 (2), 663–667.

Marks, L.S., 1951. Mechanical Engineers Handbook. . 5th ed.McGraw Hill, New York.

Misra, R.K., Rose, C.W., 1995. An examination of the relationship between erodibility parameters and soil strength. Australian Journal of Soil Research 33, 715–732.

Munoz-Carpena, R., Parsons, J.E., Gilliam, J.W., 1999. Modelling hydrology and sediment transport in vegetative filter strips. Journal of Hydrology 214, 111–129.

Samuels, P.G., 1989. Backwater length in rivers. Proceedings of Institution of Civil Engineers, Part 2, 87, December, pp. 571–581. (Paper 9479, Water Engineering Group).